Macromolecules

Article

pubs.acs.org/Macromolecules

Understanding the Interfacial Mechanical Response of Nanoscale Polymer Thin Films via Nanoindentation

Wenjie Xia,[†] Jake Song,[‡] David D. Hsu,[§] and Sinan Keten*[,†,§]

[†]Department of Civil & Environmental Engineering, [‡]Department of Materials Science & Engineering, and [§]Department of Mechanical Engineering, Northwestern University, 2145 Sheridan Road, Evanston, Illinois 60208-3109, United States

Supporting Information

ABSTRACT: Understanding the mechanical properties of interphase regions in supported polymer thin films is critical as it yields key insights into the constitutive behavior of nanostructured materials. While studies have consistently shown that polymer layers near the substrate exhibit a stiffened response, the size of this region has been reported to vary based on the measurement approach, ranging from hundreds of nanometers in atomic force microscopy (AFM) nanoindentation experiments to a few nanometers in molecular simulations and thin film wrinkling experiments. Here we employ nanoindentation simulations using a coarse-grained molecular dynamics approach to investigate the elastic moduli gradients near the substrate interface of a supported poly(methyl methacrylate) (PMMA) thin film. We find that indenter sizes commonly used in experiments give rise to observed interphase length scales that are larger than the regions in which polymer dynamics are significantly altered as quantified by the segmental molecular stiffness via the Debye−Waller factor (DWF) in simulations. We find that the measured interphase length ξ^{int} increases for larger indenter tip radii (R) and can be corroborated with the size dependence of the stress field following an $R^{1/2}$ scaling relationship. Accordingly, we show that extrapolation to vanishing R reproduces similar interphase lengths detected by the DWF. Our results elucidate possible origins of previous discrepancies in interphase measurements and suggest that the indenter tip radius and indentation depth are important factors that must be considered in measuring interphase properties with AFM.

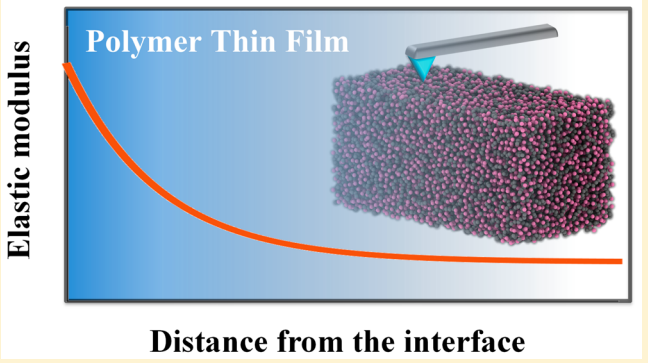

INTRODUCTION

Understanding how the material structure and chemical interfaces influence the constitutive behavior of polymer thin films has become increasingly important as advances in nanoelectronics,[1] nanocomposites,[2] coatings,[3] and biosensors[4] call for films with thicknesses less than ~100 nm. Numerous reports have ascertained a stiffened response in the chain dynamics of polymer thin films supported by attractive substrates, as manifested by an increase in the elastic modulus (E)[5] and glass transition temperature (T_g) (Figure 1a).[6] In analogy to thin films, nanofillers dispersed in polymer−nanocomposites also exhibit similar effects when the interaction between the filler and the matrix is highly favorable (Figure 1b). The quantitative similarity between these systems has been utilized in works that have studied layered models and then related their findings to nanocomposites by drawing a "thin film−nanocomposite analogy".[7−9] Therefore, a robust understanding of polymer constitutive behavior near interfaces is of critical importance in designing better thin films as well as well as nanocomposites.

Despite significant progress toward understanding the T_g and chain dynamics of polymer thin films over the past two decades, the mechanical behavior of these systems still remain to be fully understood. Several experimental techniques have been developed to assess the elastic properties of polymer thin films, such as atomic force microscopy (AFM)-based nanoindentation,[10] buckling-based metrology,[11] Brillouin light scattering (BLS),[12] beam-bending deformation,[13] and bubble AFM imaging.[14] Among these methods, AFM nanoindentation has been increasingly used to assess the dynamic and mechanical properties of nanomaterials, such as modulus and adhesion energy. One of the main advantages of this technique is its ability to resolve local property responses. However, taking the actual experimental observables such as cantilever deflection and frequency changes and correlating them with the properties of interest can be challenging at such small scales. This is because factors such as heterogeneity in materials response, adhesive interactions between the tip and polymer, and indentation depth need to be all accounted for. Additionally, accurately characterizing the indenter tip geometry and size in relation to heterogeneities in a material presents a major challenge in itself,[15] which may affect the interpretation

Received: January 18, 2016
Revised: March 23, 2016
Published: May 13, 2016

DOI: 10.1021/acs.macromol.6b00121
Macromolecules 2016, 49, 3810−3817

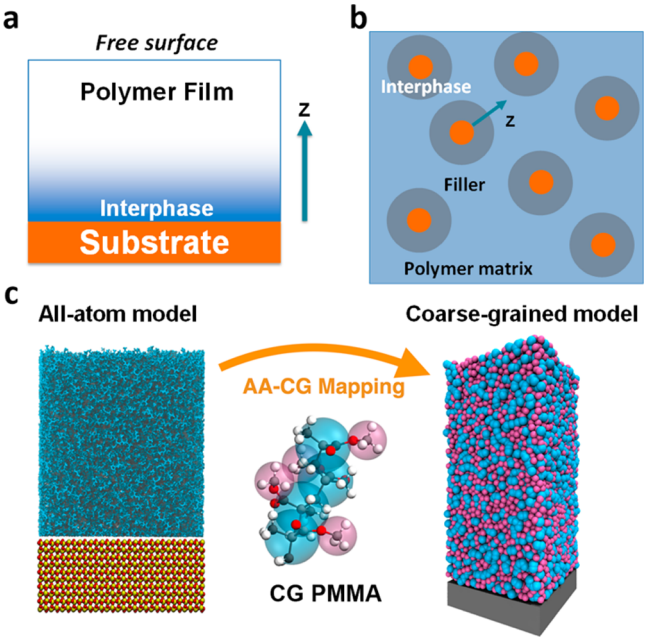

Figure 1. Illustrations of the interphase in (a) the polymer thin film near the substrate and (b) the polymer-based nanocomposite around the filler nanoparticles. (c) Mapping scheme from the all-atomistic PMMA thin film model to the coarse-grained model that is used to investigate the local elastic properties of the film.

of the measurement and limit the resolution of such studies. Given these challenges, molecular dynamics (MD) simulations[16−19] and finite element analysis (FEA)[5,20,21] offer the potential to provide valuable insights into the measured responses by carrying out computational thought experiments to reveal the relative importance of these effects.

Recently, efforts have been centralized on accurately quantifying not only the overall response of a film, where interfacial contributions will be inherently size-dependent, but also the local elastic responses near the substrate in order to characterize property gradients. In particular, considerable efforts have been directed toward characterizing the interphase length scale, ξ^{int}, which is the length scale beyond which the elastic modulus of the polymer can be considered to be approximately the same as the bulk value of the constituent polymer. Earlier studies have shown that a small change in the size of the interphase, can result in a significant change in the overall mechanical response of thin films and nanocomposites.[5,18]

Experimental investigations on polymer thin films with different measurement techniques have reported diverse results regarding the interphase length scales associated with the local mechanical responses of polymer films. In film wrinkling experiments, the elastic moduli of poly(methyl methacrylate) (PMMA) and polystyrene (PS) films supported on soft poly(dimethylsiloxane) (PDMS) substrates are observed to be lower than those of the bulk for film thicknesses ∼40 nm, possibly due to the free surface effect,[11,22] which agrees with the observations from BLS experiments.[23] In both of these studies, the thickness of the interphase in the polymer film has been estimated to be approximately several nanometers.[11,22] However, in a recent study, Cheng et al. reported interphase length scales that are much larger than those reported from film wrinkling and BLS experiments, by directly probing the local modulus of a supported PMMA film using AFM nanoindentation.[24] Indentation force measurements of ∼5 nm depth using a 10 nm radius conical indenter were taken along the lateral side of the PMMA film from the substrate to the film upper surface. Using this methodology, a gradient in the modulus as a function of distance away from the substrate could be directly obtained. The observed length scale of the interphase in their study is reported to be approximately 100 nm. The origins of these contrasting observations that have been reported by different studies remain to be further explained.

To elucidate the reasons behind these different observations, coarse-grained (CG) MD simulations can be highly useful. CG-MD can be used to perform studies on nanoscale systems at molecular resolutions, while overcoming time and length scale limitations of all-atomistic (AA) MD simulations. Here we employ our recently developed two-bead per monomer CG model for PMMA with parameters informed by AA-MD simulations.[25] As described in our previous studies, the model reproduces experimental values of key bulk properties, such as T_g, Flory−Fox constants, and the elastic modulus. In this study, we utilize our model to investigate the local elastic modulus by laterally indenting a substrate-supported film at different locations away from the substrate to map the elastic modulus profile of the mechanical interphase, in a similar vein as the recent AFM indentation experiments.[24] Our prediction of the size of mechanical interphase and its correlation with indenter tip radii and stress fields are presented and discussed.

MATERIALS AND METHODS

Coarse-Grained Model Overview. To perform nanoindentation simulations at large length and time scales, an atomistically informed CG model of atactic PMMA is used.[25] The model employs a two-bead per monomer mapping scheme, in which one bead represents the backbone group and the other represents the methyl group on the ester side chain, as shown in Figure 1c. The bonded interaction terms of the CG model are derived by applying the inverse Boltzmann method (IBM)[26] to match the bonded probability distribution of the AA PMMA system. The nonbonded interactions between all beads have been tuned to capture the temperature-dependent molecular mobility of the polymer chains in AA systems and have been shown to reproduce the elastic modulus, density, and the glass-transition temperature of atactic PMMA. This computationally efficient model speeds up the calculations by roughly 2−3 orders of magnitude compared to AA models, allowing us to perform large-scale thin film simulations that are often difficult to be simulated by AA-MD. More details of the CG model can be found in our previous publication[25] as well as subsequent works that have applied the model to thin films and nanocomposites.[19,27,28]

Configuration of the Substrate-Supported Thin Film. All CG MD simulation studies were conducted using LAMMPS.[29] The thin film system has dimensions of 40 nm × 10 nm × 100 nm on the x, y, and z axes (see Figure 2) and consists of 710 chains with 100 monomers per chain (molecular weight of 10 kg/mol). Periodic boundary conditions are applied in the y direction, and fixed boundary conditions are applied to the x and z directions. An energetic wall representing a typical substrate in experiments (such as silica) is placed in the x−y plane; it interacts with the film with the 12−6 Lennard-Jones form:

$$U_{sub}(z) = 4\varepsilon_{sp}\left[\left(\frac{\sigma_{sub}}{z}\right)^{12} - \left(\frac{\sigma_{sub}}{z}\right)^{6}\right] \quad z < z_{cut} \tag{1}$$

where z is the distance of the atoms from the substrate, σ_{sub} = 4.5 Å is the distance where U_{sub} is zero, and ε_{sp} is the potential well depth and represents the strength of the interfacial interaction between the substrate and the polymer film. In order to observe the interphase clearly in our simulations, we use a relatively large value of ε_{sp} = 5 kcal/

DOI: 10.1021/acs.macromol.6b00121
Macromolecules 2016, 49, 3810−3817

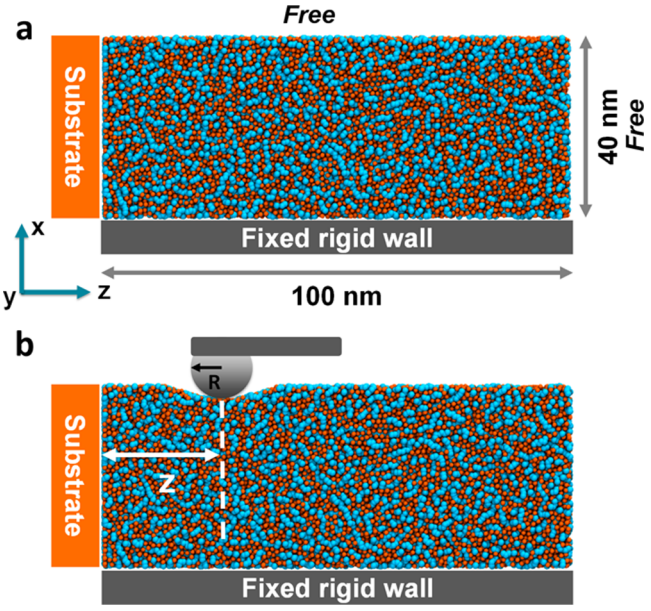

Figure 2. Snapshots of the supported coarse-grained PMMA thin film (a) initial configuration and (b) indentation simulation performed with a repulsive cylindrical indenter with a radius of R. The film size in the x direction is ~40 nm, and the z direction represents the distance away from the substrate. The indentations are performed in the direction parallel to the interface between the substrate and the film at different location along the z direction. The indenter shown here is only for illustrative purposes.

mol. This corresponds to a surface energy of ~170 mJ/m^2 that could be obtained in experiments via surface functionalization.[30] In the y–z plane, we apply another fixed rigid wall interacting with the film with the same functional form of eq 1 (by replacing variable z with x in eq 1). The ε_{sp} value of the fixed wall in the y–z plane is set to 2 kcal/mol. This is comparable to the PMMA nonbonded interaction parameter and is an intermediate value that yields neutral effects on chain dynamics based on our preliminary calculations.[19] During the equilibration process, the total energy of the system is minimized using the conjugate gradient algorithm.[31] The system is then subjected to an annealing cycle between 250 and 400 K under the NVT ensemble during the equilibration. Finally, the system is relaxed further for 2 ns at 300 K.

Indentation Simulation Setup. The overall scheme of the nanoindentation simulation is illustrated in Figure 2. A virtual rigid and smooth cylindrical indenter that extends along the y-axis and traverses the z-direction is initially placed roughly 10 Å above the thin film. The choice of using a cylindrical indenter allows us to improve computational efficiency by reducing the cross-sectional area in the x–y plane. The indenter is loaded onto the film at a constant velocity v of 5 m/s with a maximum indentation depth less than 5 nm and is then unloaded with the same velocity. This loading and unloading process is repeated along the lateral edge of the film at a variable distance z from the substrate.

From the resulting force–displacement (or indentation depth) (F–d) curves, we can calculate the local elastic modulus of the film systems. The force between the indenter and film is calculated by summing all of the repulsive forces exerted on the surface atoms according to the formula:

$$F(r) = \begin{cases} -K(r-R)^2, & r < R \\ 0, & r \geq R \end{cases} \quad (2)$$

where K is the indenter force constant, r is the distance of the atom from the center of the indenter, and R is the indenter radius. For this study, a force constant of K = 0.1 kcal/(mol Å^2) is used since it yields force magnitudes within the experimental range at small indentation depths.[24] The values of the force constant and indentation velocity used in our study have been proved to be reasonable choices based on earlier work.[32] Furthermore, we have performed characterizations which suggest that the property gradient obtained through indentation simulations are nearly independent of computationally available choices of K and v tested in our study (Figure S1 in Supporting Information). To obtain bulk results, we employ a similar system with the same dimensions in the x-, y-, and z-axis of the films and apply periodic boundary conditions in the y and z directions in order to remove the influence of the substrate.

Elastic Contact Models. The Hertz model (and its variants such as the Johnson–Kendall–Roberts (JKR) and Derjaguin–Muller–Toporov (DMT) models)[33] and the Oliver–Pharr model[10] are two branches of contact mechanics theory that are generally utilized to derive the elastic modulus from indentation experiments. In this study, we primarily derive the local elastic modulus from indentation loading curves using the classic Hertz model. Prior studies have reported the efficacy of elastic models, such as Hertz,[34] DMT,[24] and JKR[35] models, in measuring the elastic modulus of polymers at small indentation depths. One of the advantages of performing indentation simulations in MD is the availability of a rigid repulsive indenter, which eliminates external factors that may affect the accuracy of the measurement such as friction and adhesion that may otherwise be prevalent in experimental techniques. Although JKR and DMT models are commonly employed in experiments to account for these accuracy losses, the repulsive MD indenter allows us to use the Hertz contact model without losing degrees of accuracy.

The local elastic modulus is derived from the linear fit of the F–d loading curve:

$$F = \frac{\pi L E_r}{4} d \quad (3)$$

where L is the length of the cylinder (10 nm) that is set to be equal to the y dimension of the system. E_r is the reduced modulus which can be related to film elastic modulus as

$$E_r = \left(\frac{1 - \nu_{sample}^2}{E_{sample}} + \frac{1 - \nu_{tip}^2}{E_{tip}} \right)^{-1} \quad (4)$$

where ν_{sample} is the Poisson's ratio of the film. For the PMMA film sample, we use a Poisson's ratio of ~0.35, measured from tensile test simulations of the bulk system with periodic boundary conditions applied in all the directions. As mentioned above, the tip used in the simulations is a completely rigid repulsive indenter (i.e., $E_{tip} = \infty$). E_{tip} can therefore can be ignored, leading to the following expression:

$$E_r = \frac{E_{sample}}{1 - \nu_{sample}^2} \quad (5)$$

RESULTS AND DISCUSSION

To understand how material stiffness changes as a function of distance from the attractive substrate, we first evaluate force–displacement (F–d) relationships obtained during loading and unloading of the indenter. Figures 3a and 3b show typical F–d relationships that are used to determine the local elastic modulus of the film at different distances z from the interface and with different indenter tip radii R, respectively. The F–d curves in the indentation loading process exhibit well-defined linear regimes for small indentation depths (d < ~2 nm), which agrees well with the linear relationship expected from the Hertz contact model (eq 3) at small depths. The maximum Hertzian contact stresses at d = 2 nm for different indenter radii R at z = 20 nm are ~130 MPa, which are below the yield stress (σ_Y ~ 150 MPa) measured from tensile simulations[19] and also lower than that (σ_Y ~ 300 MPa) reported in experiments.[36] This

DOI: 10.1021/acs.macromol.6b00121
Macromolecules 2016, 49, 3810–3817

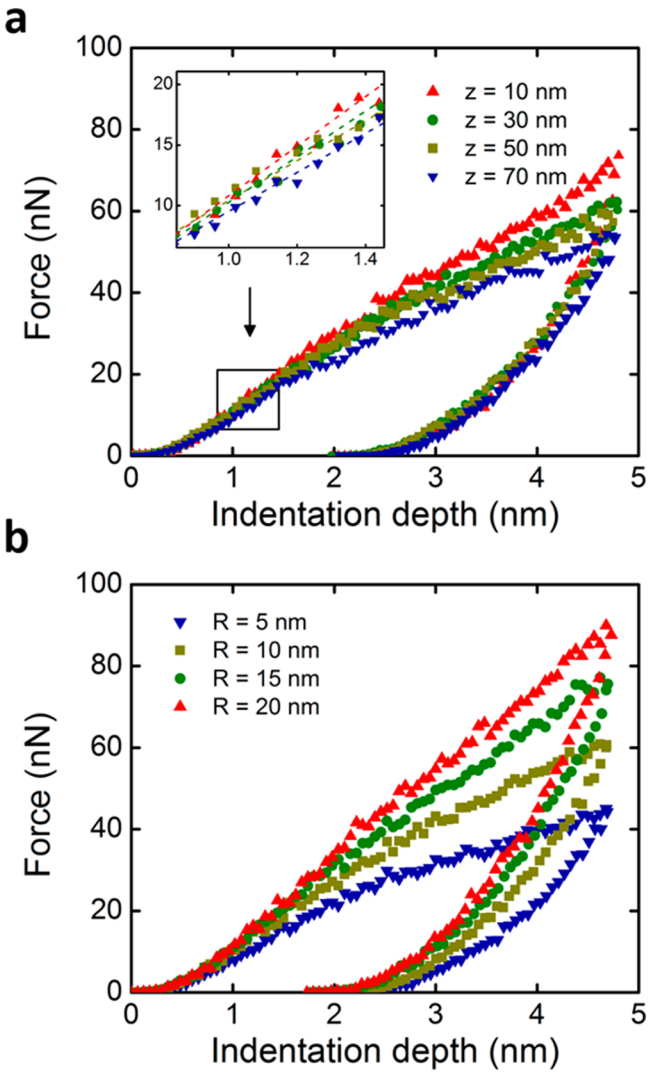

Figure 3. Typical force−indentation depth (F−d) curves obtained from nanoindentation on a PMMA thin film: (a) the F−d curves at different film positions z away from the substrate−film interface for indenter radius R = 10 nm, and F−d loading curves at small indentation depths are highlighted in the inset; (b) the F−d curves for different indenter radii R at z = 20 nm . For the Hertz model, a linear fit is obtained from the loading curve at d < 2 nm.

validates that the chosen depths are small enough to ensure elastic deformation.

The F−d curves in the unloading process corresponds well with the power law dependence as described by the Oliver−Pharr method. This suggests that both the Hertz and the Oliver−Pharr contact models are applicable for our study. However, we do not employ the Oliver−Pharr model in our study, as previous studies have shown that its unloading-based methodology may cause overestimation of the elastic modulus of soft materials.[34,37−39] Therefore, we focus primarily on applying the Hertz model, which earlier work has shown to be a good method in estimating the elastic moduli of polymers.

The different initial slopes of the F−d curves in Figure 3 clearly illustrate how the measured modulus depends on the indenter size and local film position. The progressive steepening of the F−d curve in Figure 3a as the location of indentation is moved toward the substrate can be attributed to interfacial confinement, where the mobility of the polymer chains closer to the substrate is more depressed, leading to an increase in stiffness. Using an indenter radius R = 10 nm, we observe that as the distance from the substrate z decreases from 70 to 10 nm, the measured elastic modulus normalized by the bulk (E/E_0) increases from nearly 1 to 1.18. Therefore, indenting closer to the substrate causes increased energy dissipation due to stiffening and less ductility in the polymer response. Taking the integral of the area between the loading and unloading curves in Figure 3a verifies this observation. We find the overall energy dissipated E_{diss} for z = 10, 30, 50, and 70 nm to be 3.15 × 10^4, 2.93 × 10^4, 2.78 × 10^4, and 2.51 × 10^4 kcal/mol, respectively.

Next, we examine the effects of the indenter radii on the measured modulus, as illustrated in the F−d curves in Figure 3b. As the indenter radius is increased from R = 5 nm to R = 20 nm, the normalized elastic modulus increases from about 1.04 to 1.14 at z = 20 nm. This could be attributed to the fact that larger indenter tips can cause larger stress propagation in the geometrically finite film which reaches the rigid substrate and enhance the force readings, also described as substrate effect.[20,35,40] Another interesting observation in Figure 3b is that the depth at which the softening behavior in F−d curves occurs is less for smaller indenters. For instance, the onset of softening for R = 5 nm happens at an indentation depth of about 2.5 nm, whereas there is no obvious softening for R = 20 nm. This phenomenon can be attributed to the curvature criteria in the Hertzian contact model, which necessitates that the indentation depth must be much smaller than the radius for the contact to be elastic. The sharp curvature of the smaller indenters will cause local plastic deformation at much smaller depth than those of the larger indenters, which justifies our choice of using d < 2 nm as the Hertz criterion.

Figure 4 shows the normalized local elastic modulus as a function of the distance from the substrate−polymer interface,

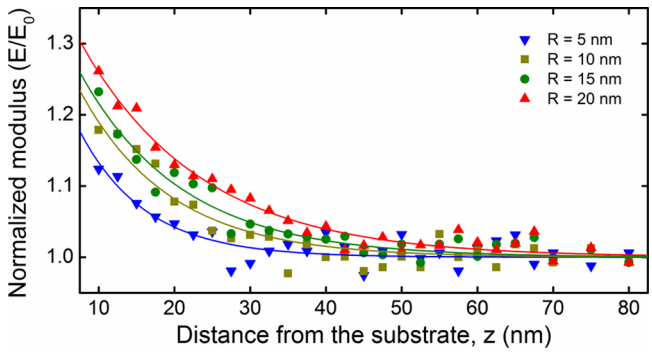

Figure 4. Profile of local elastic moduli at different distances from the substrate measured from indentation simulations with different indenter radius R. The solid lines are exponential fits (eq 6), which are used to quantify the size of the interphase length scale for different indenter sizes.

z, probed using different the indenter tip radii. The modulus profile exhibits an interphase region with enhanced apparent stiffness near the substrate compared to the bulk, which penetrates several tens of nanometers into the film interior. As the distance from the substrate increases, the local modulus decreases and converges to the bulk value. The enhancement of local mechanical properties near the substrate observed in our simulations can be attributed to the interfacial interaction and confinement effects on the local chain relaxation dynamics and mobility. At the nanoscale, due to substrate confinement and

DOI: 10.1021/acs.macromol.6b00121
Macromolecules 2016, 49, 3810−3817

strong attractive interactions with PMMA via hydrogen bond formation, the relaxation dynamics of chains near the interface are depressed significantly. This gives rise to an overall increase in elastic modulus and T_g of the films as observed in experiments. In the context of a layered composite model,[7,41] the thin film can be considered to consist of an interfacial layer with shifted properties and an interior layer with bulk-like properties, which is commonly employed to described the physics of the nanoconfinement effect. Additionally, to test whether the film size in the x direction influences the interphase characterization, we have performed the simulations on films of different sizes. Our results show that while our thin film systems do exhibit larger modulus readings with smaller sizes in the x dimension, the measured mechanical interphase remains largely independent of the film sizes (Figure S2 in Supporting Information).

As the distance from the substrate z is increased, the local modulus converges to the bulk value. The spatial variation of the normalized modulus can be empirically captured by an exponential scaling of the form:

$$\frac{E}{E_0} = 1 + A \exp\left(-\frac{z}{\xi}\right) \tag{6}$$

where A is a constant and governs the magnitude of the modulus at the interface ($z = 0$) by extrapolation, and ξ controls the rate of decay on the measured modulus as a function of the distance of the indenter from the substrate, z. A and ξ are both taken as fitting parameters that are determined from the simulation data. The mechanical interphase, characterized by the gradient of modulus as a function of distance from the substrate, is qualitatively similar to the experimental observation by Cheng et al.[24] To quantify the apparent interphase length scale ξ^{int} from the indentation measurements, we define ξ^{int} as the distance from which measured local modulus E reaches within ~1% above the polymer bulk value E_0 based on the fitting function of eq 6.

Although a similar decay of local modulus from the substrate is observed for different indenter sizes, we find that the estimated length scale of the mechanical interphase strongly depends on the indenter tip radius. Figure 5 shows the results of ξ^{int} measured from indentation as a function of $R^{1/2}$. As $R^{1/2}$ increases from ~2.2 to 4.5 $nm^{1/2}$, corresponding to indenter tip radius increases from 5 to 20 nm, the observed interphase size ξ^{int} increases from ~30 to 60 nm with an approximately linear scaling relation. This linear relation between ξ^{int} and $R^{1/2}$ can be rationalized by the Hertz contact model. Based on the Hertz model, the width of the contact area w depends on the indenter tip radius: $w = \sqrt{Rd} \sim R^{1/2}$, where d is the indentation depth. Assuming ξ^{int} linearly scales with w, one may infer the linear scaling $\xi^{int} \sim R^{1/2}$ as supported by the linear fit to the data in Figure 5. This is also in line with earlier studies that have confirmed that the measured modulus is influenced by the indenter tip radius.[21,35] Specifically, the stress field induced by the indenter can be much larger than the width of the contact area associated with the indenter tip radius, which has also been shown in the FEM simulations.[24,35] Although an analytical relationship between the indenter size and the interphase length has not been established for nanoscale polymer thin films, it is expected that the measured length scale of the interphase is strongly influenced by the stress field induced by intender tip size.

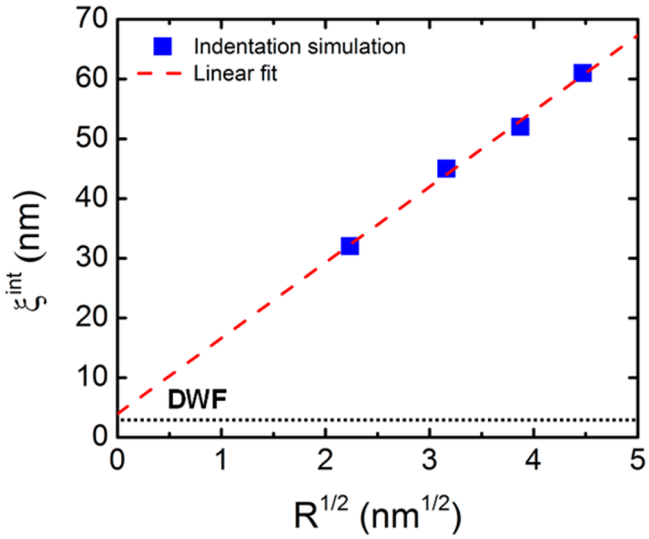

Figure 5. Measured mechanical interphase length scale ξ^{int} as a function of $R^{1/2}$ from the indentation simulations. The result of ξ^{int} is fitted with a linear slope (with an R-squared value of 0.995). As a comparison, the ξ^{int} measured from the local Debye–Waller factor (DWF) is indicated by the horizontal dotted line.

To provide mechanistic insights into the indenter size effect, we calculate the stress distribution during indentation for different indenter radii using CG-MD simulations. Figure 6 shows Von Mises stress distributions during indentation. These contour stress field plots are calculated from the atomic virial stress tensor obtained from the bonded and nonbonded interactions. As the indenter tip radius increases from 5 to 20 nm, the propagation distance of the stress field induced by the indentation also increases from ~10 to ~22 nm quantified by the average spatial stress decaying to ~20% of the maximum value, as highlighted by dashes lines in Figure 6. This distance of the stress field propagation is larger than the width of the contact region and also the corresponding indenter tip radius. The stress field comparison demonstrates that the local modulus measured from nanoindentation is an averaged value over a relatively wide range, which strongly depends on the indenter radius. Therefore, the observed mechanical interphase arises likely from the following two factors: (a) the impingement of the large stress field associated with the indenter tip radius and (b) the confinement induced change in material properties, namely the "material interphase".

Having established the dependence of interphase measurements on the indenter tip radius, we now ask the question as to what constitutes the measurement of the "true material interphase", one that has no size or geometry dependence, and only tracks changes in the local polymer properties. To better understand the elastic response of the supported film, local molecular segmental stiffness can provide physical insights into the mechanical interphase at a higher resolution. The local molecular stiffness can be assessed from MD simulations by evaluating the local Debye–Waller factor (DWF) $\langle u^2 \rangle$, which is a quantity related to thermal vibrations of atoms in a glassy solid on the order of picosecond time scales. For bead vibrations within a cage imposed by neighboring beads, the DWF can be shown to be inversely related to the local molecular stiffness: $\langle u^2 \rangle \sim k_B T/\kappa$, where k_B is the Boltzmann constant and κ is the spring constant of the local harmonic vibration which scales with the modulus. Experimentally, the

DOI: 10.1021/acs.macromol.6b00121
Macromolecules 2016, 49, 3810–3817

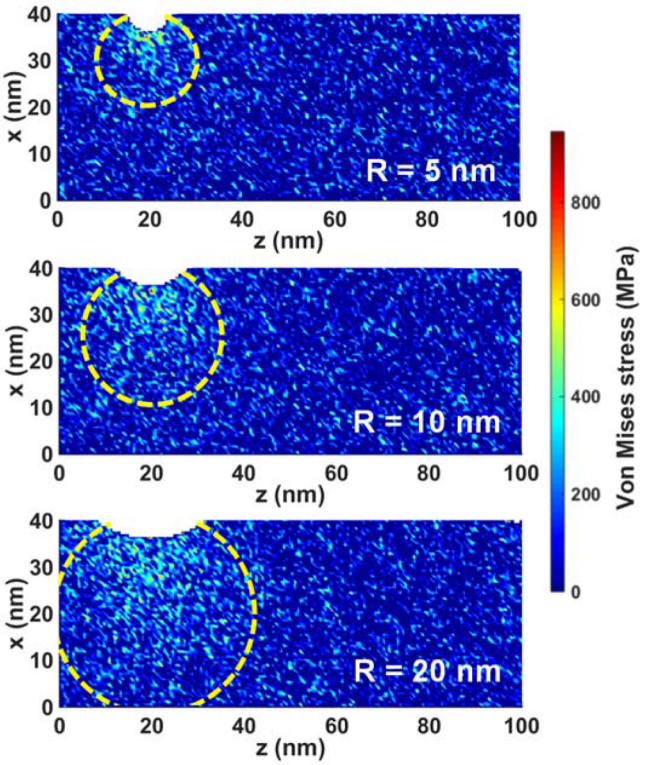

Figure 6. Comparison of the stress field (Von Mises stress) measured from the atomic virial stress tensors during nanoindentation using different indenter sizes. From top to bottom, each contour plot shows the stress field at ~20 nm away from the substrate at ~4 nm depth for the indenter radius R = 5, 10, and 20 nm, respectively. A visual illustration of the stress field has been highlighted by dashed lines to show the indenter size effects, corresponding to the average spatial stress decaying to ~20% of the maximum stress value.

DWF can be measured via incoherent neutron scattering (INS).[42,43] Previous studies have consistently shown a good correlation between the DWF and elastic properties of nanoscale polymer thin films and composites,[40,44,45] which provides confidence for using local DWF as a measurement of mechanical interphase for the glassy polymer films and also highlights the role of molecular interactions and caging effects on these systems.

In our recent work, we have utilized local DWF calculated from the local mean-squared displacement (MSD) of the atoms across the film from the substrate to quantify the size of the mechanical interphase under the influence of substrate−film interfacial interactions.[19] The result of the local DWF measurement indicated that the size of the interphase is several nanometers (shown in Figure 5 as a comparison), which is much smaller than interphase lengths reported in nanoindentation simulations and AFM experiments.[24] The length scale measured from the local DWF is larger but comparable to the length scale within which the local density is strongly perturbed due to the existence of the confining substrate and interfacial interactions.[19,46] This length scale is different from that measured by nanoindentation because, whereas DWF measures elasticity at the monomer resolution, nanoindentation samples stresses a larger activated volume that scales with R.

Considering this aspect, we next inquire whether it would be possible to obtain indentation-based mechanical interphase lengths using multiple indenter radii and extrapolate this curve to a vanishing indenter radius. Remarkably, by extrapolating the best linear fit for the scaling relationship $\xi^{int} \sim R^{1/2}$ to vanishing R yields a value for ξ^{int} that agrees well with that obtained from the DWF measurement,[19] which is indicated by the horizontal dotted line in Figure 5. This can be understood by considering that as the indenter size becomes very small and comparable to the size of monomers, the indentation will effectively act as a point load perturbation of atomic thermal vibrations, which directly probes the information on atomic caging and stiffness as measured from the DWF. Moreover, based on our previous study,[19] the size of the interphase obtained from the DWF analysis does not strongly depend on the interfacial energy, which is also evidenced by recent AFM experiments.[24] Thus, although the local modulus in this interphase region will depend on the interfacial energy, the extrapolated "material interphase" length scale will be largely interfacial energy independent. We also note that changing the percentage criteria (e.g., from 1% to 2%) to define the apparent ξ^{int} based on the fitting function of eq 6 will not change the length scale obtained by extrapolating indentation results to a vanishing R (Figure S3 in Supporting Information).

In film wrinkling experiments, the estimated thickness of the PMMA surface layer where the local elastic moduli are lower is also about several nanometers,[22] which agrees with previous simulation results based on the local stress and DWF measurements. In more recent work by Liu et al.,[47] the stress−strain response of liquid supported thin films was directly measured through tensile experiments for the first time. This experiment showed that the apparent elastic modulus of PS films decreases sharply for thicknesses below ~30 nm. This observation implies a much smaller interphase size that is roughly one order of magnitude smaller than that of the threshold thickness value,[48] which seems to be consistent with the length scale obtained from the local stress and DWF measurements.[18,19] We also note that there could be several other factors beyond the size effects discussed here that could contribute to the larger interphase lengths reported from the nanoindentation studies. A pronounced surface strengthening effect may be induced upon contact due to the adhesion force between the indenter and polymer that may also form an interphase, which may not be negligible in some experiments. As a result, the indenter may effectively act as an additional contributor to confinement and may complicate the interphase measurement. Additionally, the stiffness of underlying substrate may play a critical role in modulus and interphase measurements as suggested by Torkelson et al., who have shown that the films supported on a softer substrate exhibit a lower modulus and relaxation time.[49,50] Our work focuses on glassy polymers, but further factors may come into play above T_g due to faster relaxation dynamics and greater mobility of the polymer chains, which may influence the interphase length measurements. Future experimental and simulation studies dedicated to investigating these possible factors will help to elucidate the physical origins of the confinement effects on mechanical interphase of polymer films and explain the diverse observations in experiments.

CONCLUSION

In this work, we have employed an atomistically informed coarse-grained MD approach to investigate mechanical interphase lengths measured near attractive interfaces of supported PMMA thin films. Systematic nanoindentation simulations suggest that there exists a gradient of local modulus

DOI: 10.1021/acs.macromol.6b00121
Macromolecules 2016, 49, 3810−3817

with larger values near the substrate compared to the bulk, giving rise to interfacial confinement effects due to the substrate−film interactions. We show that the length scale of the interphase is several tens of nanometers in the case of nanoindentation measurements; however, we also show that the interphase length measurement is sensitive to indenter radii and scales with $\sim R^{1/2}$. This dependence of the measured interphase on the indenter size could be attributed to the size dependence of the stress field induced by indenters. Our result suggests that the size of the indenter tip is an important factor to consider when utilizing the indentation technique to characterize the nanoscale mechanical interphase. Our findings elucidate possible origins of discrepancies in interphase measurements between AFM indentation experiments and other approaches, and provide guidelines for better metrics such as the Debye−Waller factor (DWF) that circumvents the size dependence of measurements. Future work can build upon this finding to rigorously compare the dependence of interphase lengths on polymer and supporting substrate chemistry, adhesive forces, molecular weight, temperature, and other variables that are highly relevant for nanotechnology applications.

■ ASSOCIATED CONTENT

Supporting Information

The Supporting Information is available free of charge on the ACS Publications website at DOI: 10.1021/acs.macromol.6b00121.

Additional information on characterizations of elastic moduli and interphase (PDF)

■ AUTHOR INFORMATION

Corresponding Author

*Tel 847-491-5282; e-mail s-keten@northwestern.edu (S.K.).

Author Contributions

W.X. and J.S. contributed equally to this work.

Notes

The authors declare no competing financial interest.

■ ACKNOWLEDGMENTS

The authors acknowledge support by the University Partnership Initiative between Northwestern University and The Dow Chemical Company and by the National Institute of Standards and Technology (NIST) through the Center for Hierarchical Materials Design (CHiMaD). The authors also acknowledge support from the Department of Civil & Environmental Engineering and Mechanical Engineering at Northwestern University. A supercomputing grant from Quest HPC System at Northwestern University is acknowledged. We thank our collaborators L. Cate Brinson, John Torkelson, and Linda Broadbelt for fruitful discussions.

■ REFERENCES

(1) Ito, H. Chemical Amplification Resists for Microlithography. In *Microlithography - Molecular Imprinting*; Springer: Heidelberg, 2005; Vol. *172*, pp 37−245.

(2) Ajayan, P. M.; Schadler, L. S.; Braun, P. V. *Nanocomposite Science and Technology*; Wiley: New York, 2006.

(3) Hall, D. B.; Underhill, P.; Torkelson, J. M. *Polym. Eng. Sci.* **1998**, *38*, 2039−2045.

(4) Jianrong, C.; Yuqing, M.; Nongyue, H.; Xiaohua, W.; Sijiao, L. *Biotechnol. Adv.* **2004**, *22* (7), 505−518.

(5) Watcharotone, S.; Wood, C. D.; Friedrich, R.; Chen, X.; Qiao, R.; Putz, K.; Brinson, L. C. *Adv. Eng. Mater.* **2011**, *13* (5), 400−404.

(6) Fryer, D. S.; Peters, R. D.; Kim, E. J.; Tomaszewski, J. E.; de Pablo, J. J.; Nealey, P. F.; White, C. C.; Wu, W.-l. *Macromolecules* **2001**, *34* (16), 5627−5634.

(7) Bansal, A.; Yang, H.; Li, C.; Cho, K.; Benicewicz, B. C.; Kumar, S. K.; Schadler, L. S. *Nat. Mater.* **2005**, *4* (9), 693−698.

(8) Rittigstein, P.; Priestley, R. D.; Broadbelt, L. J.; Torkelson, J. M. *Nat. Mater.* **2007**, *6* (4), 278−282.

(9) Qin, X.; Xia, W.; Sinko, R.; Keten, S. *Nano Lett.* **2015**, *15* (10), 6738−6744.

(10) Oliver, W. C.; Pharr, G. M. *J. Mater. Res.* **2004**, *19* (1), 3−20.

(11) Stafford, C. M.; Vogt, B. D.; Harrison, C.; Julthongpiput, D.; Huang, R. *Macromolecules* **2006**, *39* (15), 5095−5099.

(12) Sun, L.; Dutcher, J. R.; Giovannini, L.; Nizzoli, F.; Stevens, J. R.; Ord, J. L. *J. Appl. Phys.* **1994**, *75* (11), 7482−7488.

(13) Delcambre, S. P.; Riggleman, R. A.; de Pablo, J. J.; Nealey, P. F. *Soft Matter* **2010**, *6* (11), 2475−2483.

(14) O'Connell, P. A.; McKenna, G. B. *Science* **2005**, *307* (5716), 1760−1763.

(15) Dokukin, M. E.; Sokolov, I. *Macromolecules* **2012**, *45* (10), 4277−4288.

(16) Yoshimoto, K.; Jain, T. S.; Nealey, P. F.; de Pablo, J. J. *J. Chem. Phys.* **2005**, *122* (14), 144712.

(17) Bohme, T. R.; de Pablo, J. J. *J. Chem. Phys.* **2002**, *116* (22), 9939−9951.

(18) Xia, W.; Keten, S. *J. Mater. Res.* **2015**, *30* (01), 36−45.

(19) Xia, W.; Keten, S. *Extreme Mech. Lett.* **2015**, *4*, 89−95.

(20) Clifford, C. A.; Seah, M. P. *Nanotechnology* **2009**, *20* (14), 145708.

(21) Clifford, C. A.; Seah, M. P. *Nanotechnology* **2006**, *17* (21), 5283−5292.

(22) Torres, J. M.; Stafford, C. M.; Vogt, B. D. *ACS Nano* **2009**, *3* (9), 2677−2685.

(23) Cheng, W.; Sainidou, R.; Burgardt, P.; Stefanou, N.; Kiyanova, A.; Efremov, M.; Fytas, G.; Nealey, P. F. *Macromolecules* **2007**, *40* (20), 7283−7290.

(24) Cheng, X.; Putz, K. W.; Wood, C. D.; Brinson, L. C. *Macromol. Rapid Commun.* **2015**, *36* (4), 391−397.

(25) Hsu, D. D.; Xia, W.; Arturo, S. G.; Keten, S. *J. Chem. Theory Comput.* **2014**, *10* (6), 2514−2527.

(26) Müller-Plathe, F. *ChemPhysChem* **2002**, *3* (9), 754−769.

(27) Qin, X.; Xia, W.; Sinko, R.; Keten, S. *Nano Lett.* **2015**, *15* (10), 6738−6744.

(28) Xia, W.; Hsu, D. D.; Keten, S. *Macromol. Rapid Commun.* **2015**, *36* (15), 1422−1427.

(29) Plimpton, S. *J. Comput. Phys.* **1995**, *117* (1), 1−19.

(30) Khoshkava, V.; Kamal, M. R. *Biomacromolecules* **2013**, *14* (9), 3155−3163.

(31) Payne, M. C.; Teter, M. P.; Allan, D. C.; Arias, T. A.; Joannopoulos, J. D. *Rev. Mod. Phys.* **1992**, *64* (4), 1045−1097.

(32) Wu, X.; Moon, R.; Martini, A. *Cellulose* **2013**, *20* (1), 43−55.

(33) Johnson, K. L. *Contact Mechanics*; Cambridge University Press: 1987.

(34) Martinez, R.; Xu, L. R. *MRS Commun.* **2014**, *4* (03), 89−93.

(35) Nguyen, H. K.; Fujinami, S.; Nakajima, K. *Polymer* **2016**, *87*, 114−122.

(36) Richeton, J.; Ahzi, S.; Vecchio, K. S.; Jiang, F. C.; Adharapurapu, R. R. *Int. J. Solids Struct.* **2006**, *43* (7−8), 2318−2335.

(37) VanLandingham, M. R.; Villarrubia, J. S.; Guthrie, W. F.; Meyers, G. F. *Macromol. Symp.* **2001**, *167* (1), 15−44.

(38) Cheng, Y. T.; Cheng, C. M. *J. Mater. Res.* **2005**, *20* (4), 1046−1053.

(39) Tranchida, D.; Piccarolo, S. *Macromol. Rapid Commun.* **2005**, *26* (22), 1800−1804.

(40) Chung, P. C.; Glynos, E.; Green, P. F. *Langmuir* **2014**, *30* (50), 15200−15205.

(41) Forrest, J. A.; Mattsson, J. *Phys. Rev. E: Stat. Phys., Plasmas, Fluids, Relat. Interdiscip. Top.* **2000**, *61*, R53−R56.

DOI: 10.1021/acs.macromol.6b00121
Macromolecules 2016, 49, 3810−3817

(42) Ye, C.; Wiener, C. G.; Tyagi, M.; Uhrig, D.; Orski, S. V.; Soles, C. L.; Vogt, B. D.; Simmons, D. S. *Macromolecules* **2015**, *48* (3), 801−808.
(43) Simmons, D. S.; Cicerone, M. T.; Zhong, Q.; Tyagi, M.; Douglas, J. F. *Soft Matter* **2012**, *8* (45), 11455−11461.
(44) Chung, P. C.; Green, P. F. *Macromolecules* **2015**, *48* (12), 3991−3996.
(45) Mangalara, J. H.; Simmons, D. S. *ACS Macro Lett.* **2015**, *4* (10), 1134−1138.
(46) Lang, R. J.; Simmons, D. S. *Macromolecules* **2013**, *46* (24), 9818−9825.
(47) Liu, Y.; Chen, Y.-C.; Hutchens, S.; Lawrence, J.; Emrick, T.; Crosby, A. J. *Macromolecules* **2015**, *48* (18), 6534−6540.
(48) Ediger, M. D.; Forrest, J. A. *Macromolecules* **2014**, *47* (2), 471−478.
(49) Evans, C. M.; Narayanan, S.; Jiang, Z.; Torkelson, J. M. *Phys. Rev. Lett.* **2012**, *109* (3), 038302.
(50) Askar, S.; Evans, C. M.; Torkelson, J. M. *Polymer* **2015**, *76*, 113−122.

DOI: 10.1021/acs.macromol.6b00121
Macromolecules 2016, 49, 3810−3817